JACS
JOURNAL OF THE AMERICAN CHEMICAL SOCIETY
Article
pubs.acs.org/JACS

Toward an Understanding of Selective Alkyne Hydrogenation on Ceria: On the Impact of O Vacancies on H_2 Interaction with $CeO_2(111)$

Kristin Werner,*[†] Xuefei Weng,[†] Florencia Calaza,[†,‡] Martin Sterrer,[§] Thomas Kropp,*[∥] Joachim Paier,[∥] Joachim Sauer,[∥] Markus Wilde,*[⊥] Katsuyuki Fukutani,[⊥] Shamil Shaikhutdinov,[†] and Hans-Joachim Freund[†]

[†]Fritz-Haber-Institut der MPG, Faradayweg 4-6, 14195 Berlin, Germany
[‡]Instituto de Desarrollo Tecnológico para la Industria Química (INTEC), UNL-CONICET, Güemes 3450, 3000 Santa Fe, Argentina
[§]Institute of Physics, University of Graz, NAWI Graz, Universitätsplatz 5, 8010 Graz, Austria
[∥]Institut für Chemie, Humboldt-Universität, Unter den Linden 6, 10099 Berlin, Germany
[⊥]Institute of Industrial Science, The University of Tokyo, 4-6-1 Komaba, Meguro-ku, 153-8505 Tokyo, Japan

Supporting Information

ABSTRACT: Ceria (CeO_2) has recently been found to be a promising catalyst in the selective hydrogenation of alkynes to alkenes. This reaction occurs primarily on highly dispersed metal catalysts, but rarely on oxide surfaces. The origin of the outstanding activity and selectivity observed on CeO_2 remains unclear. In this work, we show that one key aspect of the hydrogenation reaction—the interaction of hydrogen with the oxide—depends strongly on the presence of O vacancies within CeO_2. Through infrared reflection absorption spectroscopy on well-ordered $CeO_2(111)$ thin films and density functional theory (DFT) calculations, we show that the preferred heterolytic dissociation of molecular hydrogen on $CeO_2(111)$ requires H_2 pressures in the mbar regime. Hydrogen depth profiling with nuclear reaction analysis indicates that H species stay on the surface of stoichiometric $CeO_2(111)$ films, whereas H incorporates as a volatile species into the volume of partially reduced $CeO_{2-x}(111)$ thin films ($x \sim 1.8$–1.9). Complementary DFT calculations demonstrate that oxygen vacancies facilitate H incorporation below the surface and that they are the key to the stabilization of hydridic H species in the volume of reduced ceria.

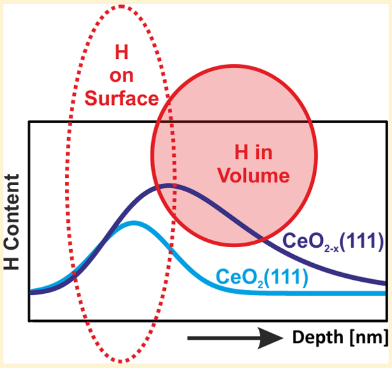

■ INTRODUCTION

Ceria (CeO_2) is one of the most extensively used oxides in heterogeneous catalysis.[1] Especially in redox reactions, CeO_2 is an efficient catalyst due to its facile oxygen store-and-release behavior. Within CeO_2, Ce^{4+} ions are easily reduced to Ce^{3+} without major structural transformations. In this way, CeO_2 can serve as an oxygen reservoir, which renders it an ideal supporting material in a variety of oxidation reactions. In contrast, applying CeO_2 as a hydrogenation catalyst may appear counterintuitive. Recently, however, CeO_2 has been found to act as a remarkable stand-alone catalyst in the selective hydrogenation of alkynes to alkenes. Pérez-Ramirez and co-workers demonstrated its excellent activity and selectivity for pentyne and acetylene semihydrogenation.[2−4] Reportedly, supported CeO_2 even outperforms commonly used Pd catalysts, which may suggest CeO_2 as a promising alternative to expensive precious metal catalysts.[3] Besides CeO_2, In_2O_3, and FeO_x have recently been reported to selectively catalyze the semihydrogenation of alkynes.[5,6] In the case of indium oxide, oxygen vacancies play a crucial role in the activation of the catalyst. At the same time, other metal oxides like ZnO or TiO_2, primarily catalyze alkyne isomerization or oligomerization reactions.[7−9] To understand the exact relation between the oxides' chemical nature and their catalytic performance toward alkyne hydrogenation, further studies are of highest interest.

The mechanism of the selective hydrogenation reaction over CeO_2 has been studied theoretically, but still needs experimental proof.[4,10] Theoretical studies on the interaction of H_2 and $CeO_2(111)$ showed that H_2 dissociates heterolytically over the Ce and O sites of the surface, which act as a Lewis acid−base pair.[11,12] With the aim of identifying the properties of CeO_2 that render it an efficient hydrogenation catalyst, we study in this work the interaction of molecular hydrogen with ceria surfaces of different O vacancy density, i.e. different degrees of reduction.

Previous work on CeO_2 catalysts suggested that the nearly stoichiometric $CeO_2(111)$ surface is more active in the selective hydrogenation reaction than the vacancy-rich $CeO_2(100)$.[13,14] This finding points toward a detrimental influence of oxygen vacancies on the hydrogenation reaction.

The apparent effect of oxygen vacancies on the hydrogenation reactivity makes it essential to study the process on atomically well-defined CeO_2 surfaces with a controlled amount

Received: September 19, 2017
Published: November 13, 2017

DOI: 10.1021/jacs.7b10021
J. Am. Chem. Soc. 2017, 139, 17608−17616

of O vacancies. The fabrication of such surfaces demands strict control over the preparation conditions, which is achieved in ultrahigh vacuum (UHV) environments, as they are typically employed in surface science. It has been reported that the dissociation of H_2 over $CeO_2(111)$ does not occur under the usual pressure limitations of UHV setups.[15,16] In consequence, previous studies on the interaction of H and well-defined CeO_2 used atomic H sources or mimicked surface hydrogenation by dissociating H_2O over reduced CeO_{2-x}.[15,17,18] Experimental work on H_2 dissociation on CeO_2 was exclusively performed on powder samples.[19−24] By studying UHV-prepared samples in a high pressure cell, we are able to study the dissociation of molecular H_2 on atomically well-defined CeO_2 surfaces.

Past studies on hydrocarbon hydrogenation over Pd model catalysts revealed the important role of absorbed H species below the surface.[25−32] In this respect, a central question of the present work is whether CeO_2 may store hydrogen below the surface as well. Previous studies addressing this question investigated powder samples and have come to controversial conlusions.[19−24] Some authors report the incorporation of H into the CeO_2 bulk,[19−22,24] while others claim that hydrogenation is a pure surface process.[23] Very recent work by Ramirez-Cuesta and co-workers suggested hydride incorporation into bulk O vacancies after H_2 dissociation on reduced CeO_{2-x}.[24] This study, however, was performed on CeO_2 rods with various surface terminations and surface defects, so that it remains unclear whether the hydrogenation-active $CeO_2(111)$ surface alone would also incorporate H. Moreover, inelastic neutron spectroscopy, which the study used to probe H in the volume of CeO_2, cannot give information about the depth distribution of H species, which would be desirable to estimate the influence of these H species on surface reactions.

In this work, to exclusively study the interaction of H_2 with $CeO_2(111)$, we make use of well-ordered $CeO_2(111)$ thin films grown on Ru(0001) as model systems. The oxygen vacancy concentration of these films can be varied in a controlled manner.[33−36] This allows us to study the role of oxygen vacancies on the interaction with H_2. We carried out hydrogen adsorption experiments using infrared reflection absorption spectroscopy (IRAS) in combination with density functional theory (DFT) calculations and examined the depth distribution of H species in the near-surface region of H_2-exposed ceria films by nuclear reaction analysis (NRA). The latter provides us with a direct probe of the spatial distribution of H species within the ceria films. We show that H_2 dissociates both on stoichiometric $CeO_2(111)$ and on reduced $CeO_{2-x}(111)$ thin films. On $CeO_2(111)$, the H species formed by dissociation predominantly stay on the surface, whereas they incorporate into the oxide film volume of reduced $CeO_{2-x}(111)$. Complementary DFT calculations suggest that the incorporation of H into the bulk of reduced ceria is closely related to the existence of O vacancies that can stabilize H as a hydridic species.

■ EXPERIMENTAL METHODS

Experiments were carried out in two UHV chambers (base pressure ~ 1×10^{-10} mbar). The first chamber in Berlin is equipped with an IR spectrometer (Bruker i66v), a LEED instrument (Specs ErLEED 1000-A), and XPS (Specs XR 50, PHOIBOS 150 MCD). We performed the in situ IRAS experiments in up to 10 mbar of D_2 (Linde, 5.0) in a built-in high pressure cell sealed by spring-loaded Teflon rings. IRA spectra were recorded with 500 scans and a spectral resolution of 4 cm^{-1}. XP spectra were recorded with Al Kα radiation in normal emission (sample normal to analyzer) and in grazing emission modes (sample 60° off-normal). Nuclear reaction analysis (NRA) measurements were performed in the second UHV chamber at the 1E beamline of the MALT accelerator at the University of Tokyo. The setup is equipped with a γ-ray scintillation detector (BGO, Oken) for NRA along with all necessary equipment for in situ sample preparation and a Pd-membrane diffusion purifier (P+E 2001) for the production of ultrapure (9N) H_2.[37]

The $CeO_2(111)$ and $CeO_{2-x}(111)$ thin films have been prepared by vapor deposition onto a Ru(0001) substrate. It has been shown previously that $CeO_2(111)$ films may be prepared on various metal substrates and that these films show essentially the same physical and chemical surface properties as bulk CeO_2.[38] Through CO dosage followed by TDS measurements (where no adsorbed CO was detectable) we carefully verified that the $CeO_2(111)$ films were fully closed, i.e., that our samples did not contain any open patches of Ru that would have been accessible from the gas phase. We may thus securely rule out H_2 dissociation and supply of atomic H to the $CeO_2(111)$ films from the substrate.

In both chambers, a Ru(0001) single crystal (MaTeck GmbH) was spot-welded to a sample holder with Ta wires. The sample was heated by resistive heating or e-beam heating and cooled with liquid N_2. The sample temperature was controlled using a type K thermocouple spot-welded to the backside or edge of the crystal. The clean Ru(0001) surface was prepared by repeated cycles of Ar^+ sputtering and UHV annealing up to 1250 K.

To grow CeO_2 films, the clean Ru(0001) surface was first exposed to 1×10^{-6} mbar of O_2 at 980 K and cooled down to 300 K to form a 3O(2 × 2)-Ru(0001) structure. Then Ce (99.9%, Sigma-Aldrich) was vapor deposited onto the 3O(2 × 2)-Ru(0001) surface in an O_2 atmosphere (1×10^{-6} mbar). Ce was evaporated from Mo crucibles in an e-beam evaporator (Focus EFM3). We ensured proper wetting of the substrate by depositing the first layers at a sample temperature of ~100 K. Then the temperature was raised to 673 K at a rate of 1 K/s (while keeping the Ce flux) and kept constant during deposition of the next layers. Deposition at 673 K was performed in cycles that included 30 to 60 min of Ce evaporation and subsequent annealing in 10^{-6} mbar O_2 at 980 K for several minutes to ensure good film ordering. LEED from the resulting films showed a hexagonal (1.4 × 1.4) pattern with respect to Ru(0001), which is characteristic for $CeO_2(111)$ due to its 40% larger lattice parameter. We estimate the thickness of the films from the attenuated Ru 3d signal in XPS to be 4−6 nm. For more details on the growth procedure, please refer to refs 39−41.

Reduced $CeO_{2-x}(111)$ thin films were prepared by UHV-annealing the $CeO_2(111)$ thin film at 1000−1200 K for 10−40 min. These films show a complex LEED pattern with a $(\sqrt{7} \times \sqrt{7})$-R19.1° superstructure of oxygen vacancies.[33,42]

As judged by LEED and XPS, the reduced film can be reoxidized to the stoichiometric $CeO_2(111)$ film in 10^{-6} mbar of O_2 at 980 K, suggesting that oxidation and reduction are fully reversible. Thus, experiments on the oxidized and reduced films can be performed with the same sample.

NRA via the resonant $^1H(^{15}N,\alpha\gamma)^{12}C$ nuclear reaction ($^{15}N + {}^1H \rightarrow {}^{12}C + \alpha + \gamma$) was used to analyze the H depth distribution in the H_2-exposed thin ceria films, using monochromatized $^{15}N^{2+}$ ion beams of 20−40 nA near the narrow (1.8 keV) reaction resonance energy, E_R = 6.385 MeV. The method is described in detail elsewhere.[37,43−46] Briefly, the γ-ray yield emitted in the nuclear reaction normalized to the number of incident ^{15}N ions quantitatively determines the density of ^1H nuclei in the sample. The ^{15}N ion current is measured with a Faraday cup on the beamline and the γ-detection efficiency was calibrated with Kapton ($(C_{22}H_{10}O_5N_2)_n$) foil as a H concentration standard. ^{15}N ions incident at E_R detect H on the sample surface, whereas those incident at higher energy ($E_R + \Delta E$) probe H underneath the surface at a depth $d = \Delta E \cos(\alpha_i)/S$. Here, S is the stopping power of the sample material for the 6.4 MeV ^{15}N ions (S = 2.6713 keV/nm for CeO_2), and α_i is the incidence angle of the ^{15}N ion beam relative to the surface normal. All measurements were performed at α_i = 60°. Scanning the ^{15}N energy through and beyond E_R reveals the depth profile of H in the sample. Due to the finite depth resolution, H within a narrow region beneath the surface cannot be distinguished from H on the surface when the incident ^{15}N energy is fixed at E_R. The thickness of this simultaneously probed region is given by the width (fwhm) of the Doppler-broadened[37] surface resonance peak, which amounts to a few O−Ce−O trilayers of CeO_2.[38]

■ COMPUTATIONAL METHODS

Calculations were performed using the projector augmented wave method (PAW)[47,48] as implemented in the Vienna ab initio simulation package (VASP).[49,50] The onsite Coulomb interaction of occupied f orbitals is corrected via the DFT+U approach[51,52] employing the functional of Perdew, Burke, and Enzerhof (PBE),[53] and an effective Hubbard-type U parameter of 4.5 eV for the Ce 4f electrons (see ref 54). While the choice of the U parameter affects reaction energies,[55] we are confident that our approach yields reliable results, which was tested by comparing with results obtained using more reliable hybrid functionals (e.g., ref 56). The specific implementation of DFT+U follows Dudarev et al.[57,58] A plane wave kinetic energy cutoff of 600 eV was used and structure optimizations were performed until forces acting on the relaxed atoms were below 0.02 eV/Å.

The $p(4 \times 4)$ surface unit cell was generated by cutting bulk CeO_2 in (111) orientation with a cell vector of 1552 pm. Our slab model consists of nine atomic layers ($Ce_{48}O_{96}$), where the lowest trilayer is frozen to simulate the bulk. The vacuum layer was set to 10 Å. Because of the large cell, sampling the Brillouin zone was restricted to the Γ point.

Optimized structures were proven to be minima by the absence of imaginary vibrational frequencies; for each transition structure, only one imaginary frequency was obtained. These calculations include all adatoms and the topmost three atomic layers. Harmonic force constants are calculated as numerical derivatives with atomic displacements of ±1.5 pm. Entropies and zero-point vibrational energies (ZPVE) are calculated from these frequencies. All energies reported herein were obtained using PBE+U and include ZPVE.

For OH (OD) stretching modes, a scaling factor of $f = 0.9773$ ($f = 0.9934$) is employed, which was derived in ref 59 as the ratio of observed fundamentals and the average of the calculated harmonic wavenumbers of the symmetric and asymmetric stretching modes of water.

Transition structures are obtained by NEB calculations[60,61] in combination with the climbing image method[62] as implemented in VASP. Four images were used for each NEB calculation with a spring force of 5 eV/Å. The improved dimer method was used to refine these structures.[63,64]

■ RESULTS

In the present work, we study well-ordered $CeO_2(111)$ and $CeO_{2-x}(111)$ thin films. Figure 1 shows typical Ce 3d XP spectra and LEED patterns of the $CeO_2(111)$ film as grown (top) and after reduction by UHV annealing (bottom). In the following, we will refer to these films as "stoichiometric" or $CeO_2(111)$ and "reduced" or $CeO_{2-x}(111)$ films, respectively. We have shown previously[40,65] that the stoichiometric films are characterized by a low density of point defects, at least on the terraces. The same holds true for the reduced films as shown in an STM study by Matolín and co-workers.[33]

The Ce 3d XP spectrum of $CeO_2(111)$ shows characteristic peaks for Ce^{4+}[38,66−70] which are commonly described in terms of three doublets. The spectra were recorded both in normal and grazing emission geometry (60° off-normal), in order to extract information on the Ce oxidation states in the bulk and at the surface of the ceria films. For CeO_2 films, the information depth in normal mode is about 3 nm, while it is about 1.5 nm in grazing mode (60°).[33]

For the $CeO_2(111)$ film, the relative intensity of the Ce 3d features is the same in grazing and normal emission geometry, indicating that the Ce ions are fully oxidized to Ce^{4+} throughout the $CeO_2(111)$ film.

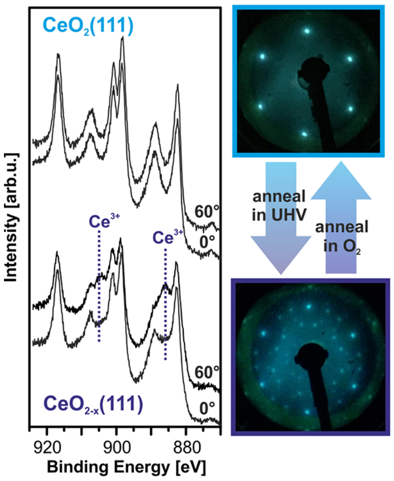

Figure 1. Ce 3d XP spectra and LEED patterns (at 102 eV) of the fully oxidized $CeO_2(111)$ (top) and reduced $CeO_{2-x}(111)$ (bottom) thin films, respectively. The spectra are recorded in normal (0°) and grazing emission (60°) geometry. The dotted lines indicate the position of the most prominent Ce^{3+} features.

The reduced $CeO_{2-x}(111)$ thin films show a complex LEED pattern with the characteristic $(\sqrt{7} \times \sqrt{7})$-R19.1° superstructure formed by O vacancies.[33] The sharpness of the LEED spots varies with the preparation conditions. Compared to stoichiometric $CeO_2(111)$, additional features appear in the XP spectra which are characteristic for the Ce^{3+} state.[33,38,66] Strong enhancement of the Ce^{3+}-related signals in the spectra recorded under grazing emission indicates that the Ce^{3+} ions are mostly located in the first few atomic layers. This finding is in full agreement with the XPS study by Matolín and co-workers, which described the film as being reduced mainly at and near the surface with a reduction gradient toward the oxidized bulk phase.[33]

From the total peak areas of the deconvoluted Ce^{3+} and Ce^{4+} signals in the Ce 3d spectrum, $A(Ce^{3+})$ and $A(Ce^{4+})$, we calculate the ratio of Ce^{3+} ions among all Ce ions as $A(Ce^{3+})/[A(Ce^{3+})+ A(Ce^{4+})]$. Taking into account the complexity of the Ce 3d spectrum and the uncertainty of the subtracted Shirley background, we estimate a maximum error of ±5%.[33,71,72] We obtain a reduction of 34% (14%) Ce^{3+} in grazing (normal) emission mode corresponding to the stoichiometry $CeO_{1.83}$ ($CeO_{1.93}$). As a single O vacancy reduces two Ce^{4+} ions to Ce^{3+}, this translates to 17% (7%) of the O sites being vacant. To estimate the depth distribution of the vacancies inside the $CeO_{2-x}(111)$ film, we followed refs 33 and 73, and assumed a simplified model of the surface, where a partially reduced $(\sqrt{7} \times \sqrt{7})$-R19.1°-$CeO_{2-x}$ layer is stacked on top of a stoichiometric CeO_2 film without intermixing. With this model, we estimate that vacancies are present up to a depth of ~0.9 nm (~3 O−Ce−O trilayers). Given that the actual system will have a reduction gradient,[33] we expect vacancies also in greater depths. For more details on the XPS analysis, please refer to the Supporting Information (section S1).

The ceria films were exposed to D_2, while IRA spectra were recorded to monitor stretching vibrations of hydroxyls, ν(OD), which we expect to appear in the case of D_2 dissociation.[11,12,74] During these experiments we took thorough precautions to avoid OD formation through D_2 dissociation at the hot filament of a nearby ion gauge, which could be observed to occur even at pressures as low as 10^{-6} mbar (Figure 2b). It is known that hot

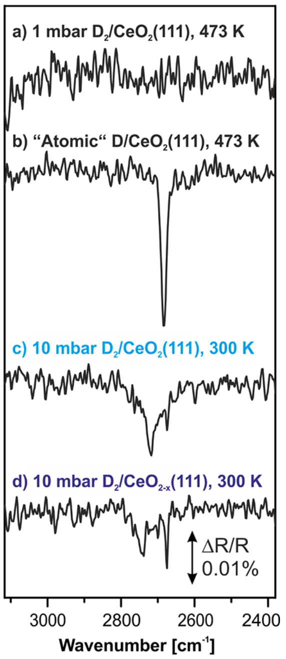

Figure 2. IRA spectra of $CeO_2(111)$ and $CeO_{2-x}(111)$ thin films exposed to D_2: (a) 1 mbar D_2 on $CeO_2(111)$ at 473 K, (b) "atomic" D on $CeO_2(111)$ at 473 K, (c) 10 mbar D_2 on $CeO_2(111)$ at 300 K, and (d) 10 mbar D_2 on $CeO_{2-x}(111)$ at 300 K.

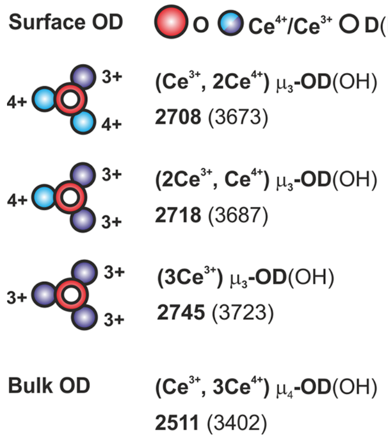

Figure 3. Scaled vibrational frequencies of surface and bulk OD (OH) groups on $CeO_2(111)$, obtained using PBE+U for structures shown schematically.

filaments may be a source of atomic D that easily hydroxylates the $CeO_2(111)$ surface.[15,17] Consequently, in order to study the interaction of *molecular* hydrogen with our ceria films, we performed the D_2/H_2 exposure experiments with all hot filaments in the vacuum system turned off.

Exposure to 1 mbar D_2 at temperatures up to 473 K did not produce any OD signals (Figure 2a). In contrast, OD species developed even at 300 K, when the D_2 pressure was increased to 10 mbar (Figure 2c). Different from the single sharp OD signal observed for atomic D on $CeO_2(111)$ (2683 cm^{-1}, Figure 2b) produced by a hot ion gauge filament for comparison, we here observe vibrations in a broad frequency range between 2800 and 2600 cm^{-1}. The signal is not symmetric, as would be expected from natural broadening of a single line. The irregular peak shape and the broadness of the feature point toward the presence of multiple OD species on or within the $CeO_2(111)$ thin film. In repeated experiments, the shape of the broad feature varied, which we interpret as a change of the intensity ratios of the different OD signals. We observe similar OD signals on the reduced $CeO_{2-x}(111)$ thin film after D_2 exposure under the same conditions (Figure 2d).

To shed light on the nature of the OD species observed by IRAS, we calculated their vibrational frequencies on a stoichiometric $CeO_2(111)$ surface by DFT. We considered three possible surface OD species that differ by the oxidation state of the coordinating Ce ions. The calculated (scaled) frequencies are summarized in Figure 3. The calculations suggest frequencies for surface OD groups between 2745 and 2708 cm^{-1}, which depend on the number of neighboring Ce^{3+} ions such that the frequency increases with the local degree of reduction. All calculated frequencies fall in the range observed experimentally. The calculations predict that OD groups formed in the CeO_2 bulk (i.e., coordinated by four Ce ions), are considerably red-shifted, i.e., to ~2510 cm^{-1}. Since we do not observe any significant intensity in this frequency range, we may safely assign the observed IRAS bands to surface OD species. The IRAS data in Figure 2 thus demonstrates that the D_2 dissociation takes place on both the stoichiometric $CeO_2(111)$ and on the reduced $CeO_{2-x}(111)$ thin films.

We next applied NRA to assess whether hydrogen species may incorporate into the ceria films upon H_2 exposure. The NRA measurements were performed after exposing the $CeO_2(111)$ and $CeO_{2-x}(111)$ films to 10 mbar of H_2 for 15 min at 300 K. We then evacuated the H_2 and obtained the NRA data at the same temperature. The results are summarized in Figure 4.

On the stoichiometric $CeO_2(111)$ film (Figure 4a), we observe a symmetric γ-yield profile of 13.6 ± 3.2 keV width (fwhm) that peaks near but not right at the surface. The slightly shifted peak position in about 0.6 ± 0.4 nm depth indicates that H species are mostly located on the surface and potentially also within a shallow region below the surface that, however, does not reach deeper than ~1.5 nm, i.e., comprises only a few oxide layers. From the integrated γ-ray intensity and our calibrated sensitivity, the total amount of H in the surface layer of the $CeO_2(111)$ thin film is evaluated to 0.5 ± 0.1 ML (one ML refers to the number of O sites on the surface of stoichiometric $CeO_2(111)$, i.e., 1 ML = 4.5×10^{14} cm^{-2}). We subsequently recorded a second H depth profile on the same sample to evaluate the possible influence of the NRA ion beam on the H distribution, as a certain degree of beam-induced H desorption may occur during the NRA analysis.[37] The second profile in Figure 4a, however, is identical to the first one within the experimental accuracy, showing that the H species in the shallow near-surface layer of oxidized $CeO_2(111)$ are rather stable. Measurements of the initial surface H signal (beam energy fixed at 6.385 MeV) as a function of the accumulated ^{15}N ion dose on freshly H_2-exposed $CeO_2(111)$ films confirm this observation (see section S2).

In contrast, for the reduced $CeO_{2-x}(111)$ film, NRA detects H species mainly near the surface but also in the film volume (see Figure 4b). Here, the first and the second NRA H profiles differ considerably. The first H profile in Figure 4b shows a broad distribution with a maximum near the surface and a large tail into the depth. The total depth-integrated γ-yield corresponds to 0.8 ± 0.1 ML of H, i.e., a substantially larger amount than that found in the surface layer of the fully oxidized, stoichiometric CeO_2 film. The depth extension, peak

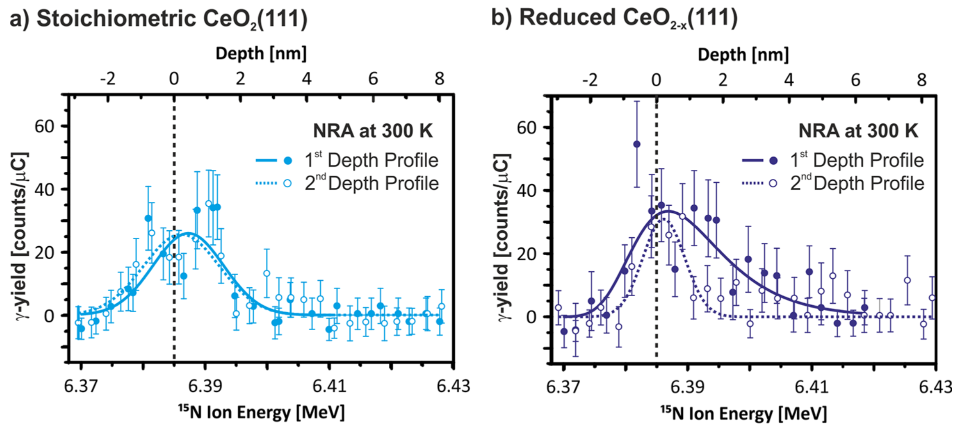

Figure 4. NRA hydrogen depth profiles obtained at 300 K after treating (a) stoichiometric $CeO_2(111)$ and (b) reduced $CeO_{2-x}(111)$ with 10 mbar H_2 at 300 K. Two subsequent profiles were recorded on both surfaces. The dotted line indicates the resonance energy of the nuclear reaction, hence, the surface position. The lines through the data are guides to the eye.

position, and asymmetric shape of the first profile from reduced $CeO_{2-x}(111)$ indicate that, in addition to surface H, the thin film contains considerable hydrogen quantities in the entire film volume, the highest H density residing closely (up to ∼1 nm depth) underneath the surface with a clear concentration gradient toward the bulk. The second scan, however, shows only a narrow (fwhm = 8.3 keV ± 1.8 keV) symmetric peak centered right at the surface with an integral γ-yield equivalent to ∼0.4 ± 0.1 ML H, i.e., less than half the amount of H detected during the first scan. These data suggest that the H species absorbed in the reduced ceria film volume are apparently much less stable against desorption by the NRA ion beam, so that they were already diminished upon acquisition of the second H profile, which only shows the remaining H on the surface. As shown in Figure S3, the fact that the H_2-exposure at 300 K builds up significant quantities of absorbed H inside the reduced CeO_{2-x} film in contrast to stoichiometric CeO_2 is confirmed with increased clarity through NRA H profiling at 200 K, where the volatile bulk-absorbed H in CeO_{2-x} is thermally slightly stabilized. Although the apparently volatile nature of H in the volume of reduced CeO_{2-x} precludes the quantitative determination of the original H content from the NRA depth profiles, the qualitative depth distribution of the absorbed H in CeO_{2-x} that peaks near the surface and shows a gradient toward the deeper film volume is clearly reproduced in the profiles of Figures 4b and S3.

■ DISCUSSION

The observation of surface OD species by IRAS (Figure 2) provides solid evidence for D_2 dissociation on both the stoichiometric $CeO_2(111)$ and the reduced $CeO_{2-x}(111)$ surfaces under the applied conditions (10 mbar, 300 K). The NRA profiles support these results, showing the presence of H species on both film surfaces.

To rationalize the experimental results, we performed a DFT study on the interaction of H_2 with $CeO_2(111)$. The results are summarized in Figure 5.

On the $CeO_2(111)$ surface (**M1**), H_2 may adsorb molecularly (**M2**) with an adsorption energy of $\Delta E_0 = -9$ kJ/mol. Starting from this adsorbed state, H_2 may dissociate homolytically or heterolytically. Along both pathways two surface hydroxyl groups form as the final product, and two Ce^{4+} ions are reduced to Ce^{3+} (**M4**). We find that the overall dissociation energy **M2** → **M4** amounts to $\Delta E_0 = -218$ kJ/mol.

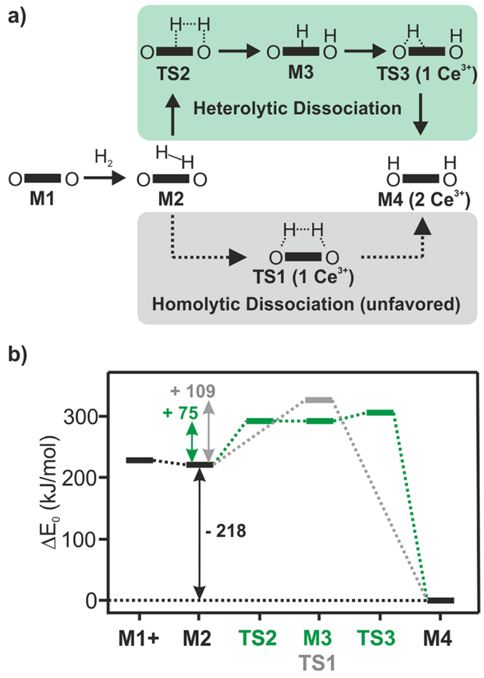

Figure 5. Theoretical (DFT) results on the dissociation of H_2 on a $CeO_2(111)$ surface. (a) Schematic representation of possible pathways. Bold lines represent Ce ions on the surface, dashed lines represent delocalized electrons. Ce ions are in oxidation state +4 if not stated otherwise. (b) Energy profile. The plus sign indicates that the reported energy includes gas phase H_2.

The homolytic dissociation pathway proceeds from the adsorbed state **M2** to the final state **M4** through transition structure **TS1** (see Figure 5). **TS1** consists of a O···H···H···O moiety. Along the imaginary mode (i.e., the vibration along the reaction coordinate; $\upsilon_i = 543$ cm^{-1}), the H−H bond is broken and the H atoms move toward the surface oxygen ions. One of the two electrons originating from the H_2 bond is localized in a Ce 4f state. The remaining electron is delocalized over the *O··· H* moiety. The activation barrier for this transition (**M2** → **TS1**) amounts to $\Delta E_0^{\ddagger} = 109$ kJ/mol. Forward relaxation of **TS1** yields the final state **M4**.

Heterolytic dissociation, in contrast, yields the same final state **M4**, but proceeds through the transition structure **TS2**, the intermediate **M3** and the transition structure **TS3**. Transition structure **TS2** (υ_i = 507 cm^{-1}) consists of an *O*⋯*H*$^+$⋯*H*$^-$⋯*Ce* moiety. The barrier for the transition **M2** → **TS2** amounts to $\Delta E_0^\ddagger$ = 75 kJ/mol, which is considerably lower than the activation barrier for homolytic dissociation (i.e., 109 kJ/mol). Forward relaxation of **TS2** leads to the intermediate structure **M3**, which consists of a protonated surface oxygen ion and a hydride coordinated to Ce^{4+} ions. The reaction energy (**M2** → **M3**) amounts to ΔE_0 = 74 kJ/mol. The energy barrier for the reverse reaction from **M3** to **TS2** is less than 1 kJ/mol, which makes the hydridic **M3** a metastable intermediate on stoichiometric $CeO_2(111)$. In a next step toward **M4**, an electron is transferred from the H$^-$ ion to a Ce 4f state, leading to transition structure **TS3**. Along the imaginary mode of **TS3** (υ_i = 331 cm^{-1}), the H atom migrates from the Ce^{3+} ion to a lattice oxygen ion with an intrinsic barrier of $\Delta E_0^\ddagger$ = 14 kJ/mol (**M3** → **TS3**). Forward relaxation from **TS3** yields **M4**. These calculated energy barriers are in good agreement with previous calculations.[11,12,75]

Overall, the energetic barriers in the heterolytic dissociation pathway are considerably smaller than the barrier in homolytic dissociation. In agreement with previous studies,[4,11,12] we therefore expect H_2 to dissociate on the $CeO_2(111)$ surface through a heterolytic pathway.

To include temperature and pressure effects, Gibbs free energies were calculated in addition (not shown in Figure 5b). The results are visualized in Figure 6, which shows a phase diagram for the states **M1**−**M4**. The creation of O vacancies through O release at high temperatures is not included in the diagram. Molecular adsorption (**M2**) is endergonic above 100 K due to entropic effects. Therefore, at T > 100 K, the overall barrier for the surface hydrogenation (**M1** → **TS3**) significantly exceeds the dissociation barrier (**M2** → **TS3**). We predict fast surface hydrogenation (k > 1 s^{-1}, i.e., a typical rate constant in temperature-programmed reduction experiments) to occur at temperatures above 600 K and at H_2 partial pressures above 0.1 mbar. The limiting pressure of 0.1 mbar to achieve H_2 dissociation exceeds by far the pressures typically used in surface science studies and thereby explains why H_2 dissociation could not be observed previously on stoichiometric $CeO_2(111)$ at lower H_2 partial pressures.[15,16]

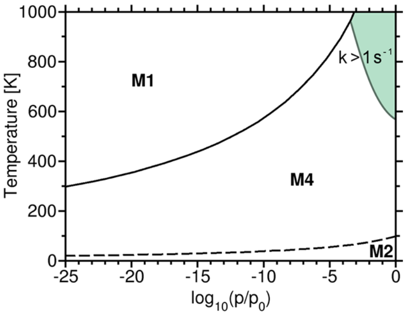

Figure 6. Phase diagram for states **M1**−**M4** in H_2 dissociation. p is the partial pressure of H_2, p_0 is the standard pressure. The area in which **M4** is formed fast (k > 1 s^{-1}) is marked in green. Efficient dissociation of molecular hydrogen only takes place at high temperatures and high pressures.

Moreover, we investigated the effect of O vacancies on the stability of surface OH groups. Therefore, we introduced a single O vacancy in the second layer (0.3 nm in depth) of the (4 × 4) CeO_2 unit cell, resulting in a vacancy density of 1/16−6% with respect to the number of O ions in pristine CeO_2. With this small density of O vacancies, the hydrogenation energy (**M1** → **M4**) changes from ΔE_0 = −227 kJ/mol on pristine $CeO_2(111)$ to ΔE_0 = −147 kJ/mol. Thus, O vacancies in the second O layer destabilize surface OH.

We further investigated whether surface OH might be transferred to the CeO_2 bulk. In principle, H species might be transferred from the surface into the bulk, where they would occupy an empty octahedral site and form an OH$^-$ species by coordinating to one of the surrounding O ions. We found, however, that such a H transfer from the surface to the second O layer is strongly endothermic, with ΔE = +154 kJ/mol per H atom. H transfer to a bulk site is even more endothermic, with ΔE = +179 kJ/mol. The overall hydrogenation energies relative to 1/2 H_2 are ΔE(1/2 H_2) = +28 kJ/mol for hydrogenation of the second O layer and ΔE(1/2 H_2) = +53 kJ/mol for bulk hydrogenation. These values are in good agreement with previously calculated hydrogenation energies.[76] We could not reproduce the exothermic bulk hydrogenation reported in an early theoretical study on H_2 dissociation over stoichiometric CeO_2.[77] In the presence of bulk O vacancies, bulk hydrogenation is slightly less endothermic, i.e., ΔE(1/2 H_2) = +39 kJ/mol. The DFT-predicted endothermic nature of bulk hydroxylation for stoichiometric CeO_2 is fully consistent with our NRA H profiles that never show appreciable H quantities in the volume of the $CeO_2(111)$ films. We disregard the possibility that the H apparently located in the shallow near-surface layer (implied by the small peak shift of ~0.5 nm in the H profiles) of the $CeO_2(111)$ films resulted from subsurface hydroxylation by H_2 dissociation on a perfectly ordered and stoichiometric $CeO_2(111)$ surface. It was noted that the size of this peak shift varied between several depth profiles taken from the same sample and sometimes (but not always) increased with the applied ^{15}N ion dose (see section S4). It is reasonable that H interacts with ion beam-induced defects in the near-surface layer. Hence, we conclude that the H_2 interaction with ideal stoichiometric $CeO_2(111)$ only produces surface hydroxyls (provided the temperature remains below the onset of associative desorption of OH as H_2O, which will in turn create O vacancies in the surface).[17]

The chemical nature of the H species found inside the reduced $CeO_{2-x}(111)$ films still needs to be clarified. Since H incorporation into the bulk of reduced CeO_{2-x} seems to depend on the presence of O vacancies that carry excess negative charge near a reduced Ce^{3+} ion, it may well be that H exists near O vacancies as a hydride species or as H_2. To investigate this possibility, we performed DFT calculations and found that H$^-$ may occupy vacant O lattice positions. While the formation of H$^-$ inside an isolated O vacancy on the surface (θ = 1/16) is endothermic with ΔE(1/2 H_2) = +76 kJ/mol, the formation of H$^-$ within an isolated bulk O vacancy is basically energy neutral (+4 kJ/mol). Thus, in the presence of O vacancies bulk H$^-$ is clearly preferred energetically over bulk OH$^-$ (ΔE(1/2 H_2) = +39 kJ/mol). Interestingly, the energies required to substitute bulk and subsurface O ions with a hydride species are similar (246 and 268 kJ/mol, respectively). Since the substitution energy is the sum of O defect formation energy and hydrogenation energy, the differences in the hydrogenation energies are a result of the different O defect formation energies for subsurface (170 kJ/mol in refs 78 and 79) and bulk (266 kJ/mol in ref 80) O ions. Thus, hydrogen destabilizes subsurface O vacancies more than bulk vacancies.

DOI: 10.1021/jacs.7b10021
J. Am. Chem. Soc. 2017, 139, 17608−17616

The weak stabilization of H^- by O vacancies in the bulk of reduced $CeO_{2-x}(111)$ naturally explains the volatile nature of the H species in the volume of our reduced $CeO_{2-x}(111)$ films that are much more susceptible to ion beam-induced desorption than surface OH on $CeO_2(111)$. The H concentration gradient from the surface toward the bulk observed in the H profiles of reduced CeO_{2-x} also suggests H-interaction with O vacancies, which are known to have a similar depth distribution.[33] Our proposed explanation is also fully consistent with a very recent inelastic neutron scattering study that reported the formation of Ce hydride species in H_2-exposed ceria nanorods.[24] Moreover, the significantly smaller fwhm of the NRA surface resonance peak in the H profiles of $CeO_{2-x}(111)$ (~9 keV) compared to $CeO_2(111)$ (13−15 keV) (see section S5) may be an indication for a different chemical nature of the probed H species in the two cases—mostly hydroxyls on $CeO_2(111)$ and mostly hydride on $CeO_{2-x}(111)$. Further experiments to clarify the chemical identity of the surface H species on $CeO_2(111)$ and $CeO_{2-x}(111)$ films are underway and will be reported elsewhere. Furthermore, studies on the interaction of H_2 with $CeO_{2-x}(111)$ films of variable oxygen vacancy concentration would be highly desirable to gain a comprehensive understanding of the underlying chemistry, as it has been demonstrated for comparable oxide systems.[81,82]

In summary, both our experimental and theoretical results show that O vacancies on $CeO_2(111)$ are crucial for its interaction with H_2. This finding might explain why previous studies came to contradicting conclusions on whether H species may dissolve into CeO_2.[19−24] These studies investigated powder samples, which typically exhibit a high concentration of defects, such as O vacancies. The nature and the concentration of these vacancies will vary considerably with the sample preparation, thus affecting the interaction with H_2. Moreover, our study hints at the possibility that chemically different hydrogen species exist on and within stoichiometric $CeO_2(111)$ as opposed to reduced $CeO_{2-x}(111)$ films. As surface OH has been predicted to be part of the rate-determining transition state for alkyne hydrogenation on CeO_2 at large H coverage,[10] this might give an important clue to understand the negative influence of oxygen vacancies on the catalytic activity of partially reduced ceria in the selective semihydrogenation of alkynes.

CONCLUSIONS

We investigated the interaction of H_2 with well-defined stoichiometric $CeO_2(111)$ and reduced $CeO_{2-x}(111)$ thin films through IR spectroscopy and NRA and found that H_2 only dissociates at elevated pressures in the mbar regime. On the fully oxidized $CeO_2(111)$ surface, H species formed by H_2 dissociation are primarily located on the oxide surface as hydroxyls. For the reduced $CeO_{2-x}(111)$ thin films, H is also found in appreciable quantities in the entire ceria volume. On the basis of DFT calculations and the shape of the H depth profile that mimics the O vacancy distribution, we propose that O vacancies stabilizing H in the form of hydride species in the oxide bulk are crucial for the incorporation of H in the interior of reduced CeO_{2-x} films.

We believe that our findings provide an important impetus to understand the reactivity of CeO_2 in selective alkyne hydrogenation reactions. Reactivity studies on $CeO_2(111)$ thin film model catalysts with controlled O vacancy densities are under way.

ASSOCIATED CONTENT

Supporting Information

The Supporting Information is available free of charge on the ACS Publications website at DOI: 10.1021/jacs.7b10021.

Details on XPS evaluation, NRA decay curves, additional NRA H profiles, beam-induced shifts in NRA profiles, NRA resonance peak widths, and theoretical simulations (PDF)

AUTHOR INFORMATION

Corresponding Authors

*werner@fhi-berlin.mpg.de
*kroppthо@chemie.hu-berlin.de
*wilde@iis.u-tokyo.ac.jp

ORCID

Kristin Werner: 0000-0001-9540-6692
Martin Sterrer: 0000-0001-9089-9061
Joachim Sauer: 0000-0001-6798-6212
Shamil Shaikhutdinov: 0000-0001-9612-9949
Hans-Joachim Freund: 0000-0001-5188-852X

Notes

The authors declare no competing financial interest.

ACKNOWLEDGMENTS

This work has been supported by the German Research Foundation (CRC 1109), COST action CM1104. H.-J.F. thanks "Fonds der Chemischen Industrie" for support. The authors are grateful for computing time at the high-performance computer centers HLRN (North-German Supercomputing Alliance). F.C. and T.K. are grateful for financial support from the Alexander von Humboldt Foundation. K.W. is a member of the IMPRS Functional Interfaces in Physics and Chemistry and is supported through a grant by the DFG-NSFC (No. FR554/18-1).

REFERENCES

(1) Sun, C. W.; Li, H.; Chen, L. Q. *Energy Environ. Sci.* **2012**, *5*, 8475.
(2) Vilé, G.; Bridier, B.; Wichert, J.; Pérez-Ramírez, J. *Angew. Chem., Int. Ed.* **2012**, *51*, 8620.
(3) Vilé, G.; Wrabetz, S.; Floryan, L.; Schuster, M. E.; Girgsdies, F.; Teschner, D.; Pérez-Ramírez, J. *ChemCatChem* **2014**, *6*, 1928.
(4) Carrasco, J.; Vilé, G.; Fernández-Torre, D.; Pérez, R.; Pérez-Ramírez, J.; Ganduglia-Pirovano, M. V. *J. Phys. Chem. C* **2014**, *118*, 5352.
(5) Albani, D.; Capdevila-Cortada, M.; Vilé, G.; Mitchell, S.; Martin, O.; López, N.; Pérez-Ramírez, J. *Angew. Chem., Int. Ed.* **2017**, *56*, 10755.
(6) Tejeda-Serrano, M.; Cabrero-Antonino, J. R.; Mainar-Ruiz, V.; López-Haro, M.; Hernández-Garrido, J. C.; Calvino, J. J.; Leyva-Pérez, A.; Corma, A. *ACS Catal.* **2017**, *7*, 3721.
(7) Pierce, K. G.; Barteau, M. A. *J. Phys. Chem.* **1994**, *98*, 3882.
(8) Nakajima, T.; Sonoda, T.; Miyata, H.; Kubokawa, Y. *J. Chem. Soc., Faraday Trans. 1* **1982**, *78*, 555.
(9) Halliday, M. M.; Kemball, C.; Leach, H. F. *J. Chem. Soc., Faraday Trans. 1* **1974**, *70*, 1743.
(10) García-Melchor, M.; Bellarosa, L.; López, N. *ACS Catal.* **2014**, *4*, 4015.
(11) García-Melchor, M.; López, N. *J. Phys. Chem. C* **2014**, *118*, 10921.
(12) Negreiros, F. R.; Camellone, M. F.; Fabris, S. *J. Phys. Chem. C* **2015**, *119*, 21567.
(13) Vilé, G.; Colussi, S.; Krumeich, F.; Trovarelli, A.; Pérez-Ramírez, J. *Angew. Chem., Int. Ed.* **2014**, *53*, 12069.

(14) Huang, W.; Gao, Y. *Catal. Sci. Technol.* **2014**, *4*, 3772.

(15) Shahed, S. M. F.; Hasegawa, T.; Sainoo, Y.; Watanabe, Y.; Isomura, N.; Beniya, A.; Hirata, H.; Komeda, T. *Surf. Sci.* **2014**, *628*, 30.

(16) Xu, J.; Overbury, S. H. *J. Catal.* **2004**, *222*, 167.

(17) Chen, B.; Ma, Y.; Ding, L.; Xu, L.; Wu, Z.; Yuan, Q.; Huang, W. *J. Phys. Chem. C* **2013**, *117*, 5800.

(18) Mullins, D. R.; Albrecht, P. M.; Chen, T.-L.; Calaza, F. C.; Biegalski, M. D.; Christen, H. M.; Overbury, S. H. *J. Phys. Chem. C* **2012**, *116*, 19419.

(19) Badri, A.; Binet, C.; Lavalley, J.-C. *J. Chem. Soc., Faraday Trans.* **1996**, *92*, 4669.

(20) Laachir, A.; Perrichon, V.; Badri, A.; Lamotte, J.; Catherine, E.; Lavalley, J. C.; El Fallah, J.; Hilaire, L.; Le Normand, F.; Quemere, E.; Sauvion, G. N.; Touret, O. *J. Chem. Soc., Faraday Trans.* **1991**, *87*, 1601.

(21) Perrichon, V.; Laachir, A.; Abouarnadasse, S.; Touret, O.; Blanchard, G. *Appl. Catal., A* **1995**, *129*, 69.

(22) Fierro, J. L. G.; Soria, J.; Sanz, J.; Rojo, J. M. *J. Solid State Chem.* **1987**, *66*, 154.

(23) Bernal, S.; Calvino, J. J.; Cifredo, G. A.; Gatica, J. M.; Omil, J. A. P.; Pintado, J. M. *J. Chem. Soc., Faraday Trans.* **1993**, *89*, 3499.

(24) Wu, Z.; Cheng, Y.; Tao, F.; Daemen, L.; Foo, G. S.; Nguyen, L.; Zhang, X.; Beste, A.; Ramirez-Cuesta, A. J. *J. Am. Chem. Soc.* **2017**, *139*, 9721.

(25) Teschner, D.; Borsodi, J.; Kis, Z.; Szentmiklósi, L.; Révay, Z.; Knop-Gericke, A.; Schlögl, R.; Torres, D.; Sautet, P. *J. Phys. Chem. C* **2010**, *114*, 2293.

(26) Teschner, D.; Borsodi, J.; Wootsch, A.; Révay, Z.; Hävecker, M.; Knop-Gericke, A.; Jackson, S. D.; Schlögl, R. *Science* **2008**, *320*, 86.

(27) Wilde, M.; Fukutani, K.; Ludwig, W.; Brandt, B.; Fischer, J.-H.; Schauermann, S.; Freund, H.-J. *Angew. Chem., Int. Ed.* **2008**, *47*, 9289.

(28) Aleksandrov, H. A.; Kozlov, S. M.; Schauermann, S.; Vayssilov, G. N.; Neyman, K. M. *Angew. Chem., Int. Ed.* **2014**, *53*, 13371.

(29) Savara, A.; Ludwig, W.; Dostert, K.-H.; Schauermann, S. *J. Mol. Catal. A: Chem.* **2013**, *377*, 137.

(30) Ludwig, W.; Savara, A.; Dostert, K.-H.; Schauermann, S. *J. Catal.* **2011**, *284*, 148.

(31) Ludwig, W.; Savara, A.; Schauermann, S. *Dalton Trans.* **2010**, *39*, 8484.

(32) Ohno, S.; Wilde, M.; Mukai, K.; Yoshinobu, J.; Fukutani, K. *J. Phys. Chem. C* **2016**, *120*, 11481.

(33) Duchoň, T.; Dvořák, F.; Aulická, M.; Stetsovych, V.; Vorokhta, M.; Mazur, D.; Veltruská, K.; Skála, T.; Mysliveček, J.; Matolínová, I.; Matolín, V. *J. Phys. Chem. C* **2014**, *118*, 357.

(34) Stetsovych, V.; Pagliuca, F.; Dvořák, F.; Duchoň, T.; Vorokhta, M.; Aulická, M.; Lachnitt, J.; Schernich, S.; Matolínová, I.; Veltruská, K.; Skála, T.; Mazur, D.; Mysliveček, J.; Libuda, J.; Matolín, V. *J. Phys. Chem. Lett.* **2013**, *4*, 866.

(35) Duchoň, T.; Dvořák, F.; Aulická, M.; Stetsovych, V.; Vorokhta, M.; Mazur, D.; Veltruská, K.; Skála, T.; Mysliveček, J.; Matolínová, I.; Matolín, V. *J. Phys. Chem. C* **2014**, *118*, 5058.

(36) Barth, C.; Laffon, C.; Olbrich, R.; Ranguis, A.; Parent, P.; Reichling, M. *Sci. Rep.* **2016**, *6*, 21165.

(37) Wilde, M.; Fukutani, K. *Surf. Sci. Rep.* **2014**, *69*, 196.

(38) Mullins, D. R. *Surf. Sci. Rep.* **2015**, *70*, 42.

(39) Baron, M.; Bondarchuk, O.; Stacchiola, D.; Shaikhutdinov, S.; Freund, H. J. *J. Phys. Chem. C* **2009**, *113*, 6042.

(40) Lu, J. L.; Gao, H. J.; Shaikhutdinov, S.; Freund, H. J. *Surf. Sci.* **2006**, *600*, 5004.

(41) Mullins, D. R.; Radulovic, P. V.; Overbury, S. H. *Surf. Sci.* **1999**, *429*, 186.

(42) Wilkens, H.; Schuckmann, O.; Oelke, R.; Gevers, S.; Schaefer, A.; Bäumer, M.; Zoellner, M. H.; Schroeder, T.; Wollschläger, J. *Appl. Phys. Lett.* **2013**, *102*, 111602.

(43) Wilde, M.; Fukutani, K.; Naschitzki, M.; Freund, H. J. *Phys. Rev. B: Condens. Matter Mater. Phys.* **2008**, *77*, 113412.

(44) Fukutani, K.; Wilde, M.; Ogura, S. *Chem. Rec.* **2017**, *17*, 233.

(45) Wilde, M.; Ohno, S.; Ogura, S.; Fukutani, K.; Matsuzaki, H. *J. Visualized Exp.* **2016**, e53452.

(46) Traeger, F.; Kauer, M.; Wöll, C.; Rogalla, D.; Becker, H. W. *Phys. Rev. B: Condens. Matter Mater. Phys.* **2011**, *84*, 075462.

(47) Blöchl, P. E. *Phys. Rev. B: Condens. Matter Mater. Phys.* **1994**, *50*, 17953.

(48) Kresse, G.; Joubert, D. *Phys. Rev. B: Condens. Matter Mater. Phys.* **1999**, *59*, 1758.

(49) Kresse, G.; Furthmüller, J. *Phys. Rev. B: Condens. Matter Mater. Phys.* **1996**, *54*, 11169.

(50) Kresse, G.; Furthmüller, J. *Comput. Mater. Sci.* **1996**, *6*, 15.

(51) Liechtenstein, A. I.; Anisimov, V. I.; Zaanen, J. *Phys. Rev. B: Condens. Matter Mater. Phys.* **1995**, *52*, R5467.

(52) Anisimov, V. I.; Zaanen, J.; Andersen, O. K. *Phys. Rev. B: Condens. Matter Mater. Phys.* **1991**, *44*, 943.

(53) Perdew, J. P.; Burke, K.; Ernzerhof, M. *Phys. Rev. Lett.* **1996**, *77*, 3865.

(54) Fabris, S.; Vicario, G.; Balducci, G.; de Gironcoli, S.; Baroni, S. *J. Phys. Chem. B* **2005**, *109*, 22860.

(55) Capdevila-Cortada, M.; Łodziana, Z.; López, N. *ACS Catal.* **2016**, *6*, 8370.

(56) Kropp, T.; Paier, J.; Sauer, J. *J. Am. Chem. Soc.* **2014**, *136*, 14616.

(57) Dudarev, S. L.; Botton, G. A.; Savrasov, S. Y.; Humphreys, C. J.; Sutton, A. P. *Phys. Rev. B: Condens. Matter Mater. Phys.* **1998**, *57*, 1505.

(58) Bengone, O.; Alouani, M.; Blöchl, P.; Hugel, J. *Phys. Rev. B: Condens. Matter Mater. Phys.* **2000**, *62*, 16392.

(59) Dementyev, P.; Dostert, K.-H.; Ivars-Barceló, F.; O'Brien, C. P.; Mirabella, F.; Schauermann, S.; Li, X.; Paier, J.; Sauer, J.; Freund, H.-J. *Angew. Chem., Int. Ed.* **2015**, *54*, 13942.

(60) Mills, G.; Jónsson, H.; Schenter, G. K. *Surf. Sci.* **1995**, *324*, 305.

(61) Jónsson, H.; Mills, G.; Jacobsen, K. W. In *Classical and Quantum Dynamics in Condensed Phase Simulations*; Berne, B. J., Cicotti, G., Coker, D. F., Eds.; World Scientific: Singapore, 1998; p 385.

(62) Henkelman, G.; Uberuaga, B. P.; Jónsson, H. *J. Chem. Phys.* **2000**, *113*, 9901.

(63) Henkelman, G.; Jónsson, H. *J. Chem. Phys.* **1999**, *111*, 7010.

(64) Heyden, A.; Bell, A. T.; Keil, F. J. *J. Chem. Phys.* **2005**, *123*, 224101.

(65) Pan, Y.; Cui, Y.; Stiehler, C.; Nilius, N.; Freund, H.-J. *J. Phys. Chem. C* **2013**, *117*, 21879.

(66) Pfau, A.; Schierbaum, K. D. *Surf. Sci.* **1994**, *321*, 71.

(67) Krawczyk, M.; Holdynski, M.; Lisowski, W.; Sobczak, J. W.; Jablonski, A. *Appl. Surf. Sci.* **2015**, *341*, 196.

(68) Mullins, D. R.; Overbury, S. H.; Huntley, D. R. *Surf. Sci.* **1998**, *409*, 307.

(69) Nelin, C. J.; Bagus, P. S.; Ilton, E. S.; Chambers, S. A.; Kuhlenbeck, H.; Freund, H. J. *Int. J. Quantum Chem.* **2010**, *110*, 2752.

(70) Bagus, P. S.; Nelin, C. J.; Ilton, E. S.; Baron, M.; Abbott, H.; Primorac, E.; Kuhlenbeck, H.; Shaikhutdinov, S.; Freund, H. J. *Chem. Phys. Lett.* **2010**, *487*, 237.

(71) Pagliuca, F.; Luches, P.; Valeri, S. *Surf. Sci.* **2013**, *607*, 164.

(72) Lykhach, Y.; Kozlov, S. M.; Skala, T.; Tovt, A.; Stetsovych, V.; Tsud, N.; Dvorak, F.; Johanek, V.; Neitzel, A.; Myslivecek, J.; Fabris, S.; Matolin, V.; Neyman, K. M.; Libuda, J. *Nat. Mater.* **2016**, *15*, 284.

(73) Wang, G. D.; Kong, D. D.; Pan, Y. H.; Pan, H. B.; Zhu, J. F. *Appl. Surf. Sci.* **2012**, *258*, 2057.

(74) Vicario, G.; Balducci, G.; Fabris, S.; de Gironcoli, S.; Baroni, S. *J. Phys. Chem. B* **2006**, *110*, 19380.

(75) Fernández-Torre, D.; Carrasco, J.; Ganduglia-Pirovano, M. V.; Pérez, R. *J. Chem. Phys.* **2014**, *141*, 014703.

(76) Wu, X. P.; Gong, X. Q.; Lu, G. *Phys. Chem. Chem. Phys.* **2015**, *17*, 3544.

(77) Sohlberg, K.; Pantelides, S. T.; Pennycook, S. J. *J. Am. Chem. Soc.* **2001**, *123*, 6609.

(78) Pan, Y.; Nilius, N.; Freund, H.-J.; Paier, J.; Penschke, C.; Sauer, J. *Phys. Rev. Lett.* **2013**, *111*, 206101.

(79) Pan, Y.; Nilius, N.; Freund, H.-J.; Paier, J.; Penschke, C.; Sauer, J. *Phys. Rev. Lett.* **2015**, *115*, 269901.

(80) Kropp, T.; Paier, J. *J. Phys. Chem. C* **2015**, *119*, 23021.

(81) Wu, Z.; Zhang, W.; Xiong, F.; Yuan, Q.; Jin, Y.; Yang, J.; Huang, W. *Phys. Chem. Chem. Phys.* **2014**, *16*, 7051.

(82) Xu, L.; Zhang, W.; Zhang, Y.; Wu, Z.; Chen, B.; Jiang, Z.; Ma, Y.; Yang, J.; Huang, W. *J. Phys. Chem. C* **2011**, *115*, 6815.